PHYSICAL REVIEW D **96,** 022003 (2017)

Crackling noise in advanced gravitational wave detectors: A model of the steel cantilevers used in the test mass suspensions

G. Vajente*

California Institute of Technology, LIGO Laboratory MC 100-36, 1200 E. California Boulevard, Pasadena, California 91125, USA

(Received 24 April 2017; published 11 July 2017)

The response of elastic materials to external changing conditions can proceed through small and discrete releases of stress, rather than a continuous and smooth deformation as described by the classical elasticity theory. In a macroscopic elastic body, the sum of all those small *crackling events* can create a detectable displacement noise (*crackling noise*). In this paper we consider the case of the steel cantilevers used in the seismic isolation systems of ground based gravitational wave detectors, to provide the vertical isolation needed to reach the detector target sensitivity. Those instruments are reaching unprecedented displacement sensitivity, at a level that might be limited by crackling noise in the aforementioned cantilevers. Understanding this source of noise is extremely important, especially considering its intrinsic nonlinear nature. Since a detailed microscopical model of crackling noise in polycrystalline steel is not available at the moment, we suggest a phenomenological microscopical model, and the focus of this paper is on how crackling noise scales with the size and geometry of the cantilevers. The goal of this paper is to provide a method to scale up future measurements of crackling noise from small test cantilevers to the large ones used in advanced gravitational wave detectors.

DOI: 10.1103/PhysRevD.96.022003

I. INTRODUCTION

The classical theory of elastic bodies treats the response to varying external forces as continuous and smooth. However, this description, while valid on average at a macroscopic scale, is not correct at the microscopic scale. Recent experiments showed that plastic deformation is actually the result of a large number of discrete events, mainly due to dislocation movements. We will call those single events *crackling*. Especially when the elastic material is stressed close to its yield point, it has been shown experimentally that large crackling events can occur [1–4]. This phenomenon, often referred to as *creep* has been studied in the design phases of the seismic isolation system of the Virgo, TAMA, and GEO600 seismic isolation system [5–7]. It has been shown experimentally that creep is largely reduced after the first loading cycles of the material [1]. Moreover, a proper choice of the material used in the suspension can also largely reduce the rate and intensity of the crackling or creep events. Experimental studies showed that maraging steel was the best candidate for this use [8–10]. Additionally, very low frequency deviations from linear elasticity have been observed experimentally [11]. We would like to stress that all the studies cited above are focused either on single, isolated loud events or on very low frequency deviations from linearity.

In this paper we are interested in a different regime of crackling, namely the possibility of a large number of small crackling events even when the material is loaded far from the yield point. Such events would not have been detected by any of the cited experiments, due to limits in their sensitivity. If a large number of such crackling events occurs in a material, it is possible to detect the collective response of the elastic system in the form of an incoherent *crackling noise*; see for example [12] for a review. The properties of this crackling noise are believed to follow some universality classes, although the details can vary from material to material.

Several experiments have been carried out to study the statistical properties of crackling noise. To the best of our knowledge, all of them were limited to microscopic systems [13,14] or aimed at the detection of single crackling events [15–17]. The theoretical understanding of crackling focused mainly on the prediction of general statistical properties of the size and time distribution, using mean field theory approaches [18] or microscopical numerical simulations [19]. In particular it is widely accepted that the amplitude and properties of the crackling noise can depend on the static stress applied to the material, as well as on the stress rate [11,20]. However, again to the best of our knowledge, there are no quantitative models of the expected crackling noise in materials like steel. Moreover, the focus of most of the experimental and theoretical work is on the plastic regime, when metals are stressed to near the yield point. Our interest is instead in the elastic regime, with stress close to 50% of the yield, since this is the operating condition of the cantilever springs used in the mirror suspensions of gravitational wave detectors [5,21,22]. Recent experimental and theoretical studies [23] have shown a deviation from the simple elastic behavior in copper nano pillars, indicating the possibility

*vajente@caltech.edu

that crackling noise can arise even in systems far from the yield point.

In this paper we consider a different approach, looking neither for single crackling events nor for low frequency deviations from linearity. The idea is to detect the collective result of all the crackling events in a macroscopic system. The motivation can be found in the use of maraging steel [24] cantilever springs (called *blades* below) in the seismic isolation systems and mirror suspensions of advanced gravitational wave detectors, such as Advanced LIGO [25], KAGRA [26], and Advanced Virgo [27]. Those detectors are designed to observe gravitational waves, by means of extremely sensitive interferometric measurements of the horizontal displacement of kg-scale test masses. Those test masses must be carefully isolated, in both horizontal and vertical directions, from ground motion, by means of sophisticated active and passive seismic isolation systems [5,21,22]. Any noise in excess of thermal noise will reduce the detector sensitivity (at the relevant frequencies above 10 Hz) and must be carefully understood and mitigated. Moreover, this excess noise can be nonstationary, being modulated by low frequency residual seismic motion.

The goal of this work is not to develop a microscopical model of crackling noise, based on *ab initio* simulations or extrapolating from experimental data. Instead, we try to develop a phenomenological model that allows us to encapsulate the way crackling noise scales with the geometry and the size of the elastic system in consideration. Studies similar to the one reported in this paper have been carried out previously, focusing mainly on the steel wires or the fused silica fibers that are used to suspend the test masses [1,28]. In this paper we focus on the cantilever springs which are used in the Advanced LIGO suspension system (Fig. 1). An example of such blades is shown in Fig. 2. A trapezoidal

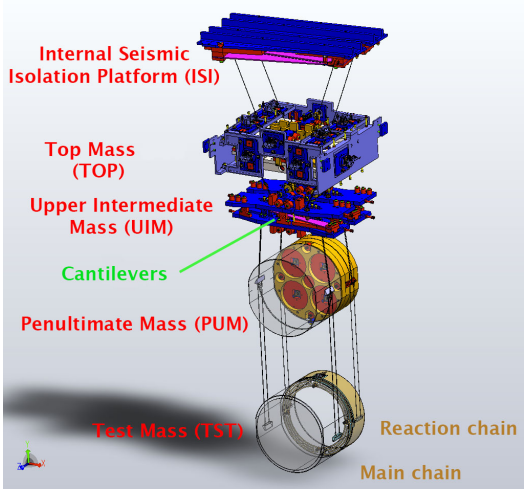

FIG. 1. Simplified scheme of the quadruple suspension system. The cantilevers being analyzed in this paper are those in the upper intermediate mass (UIM).

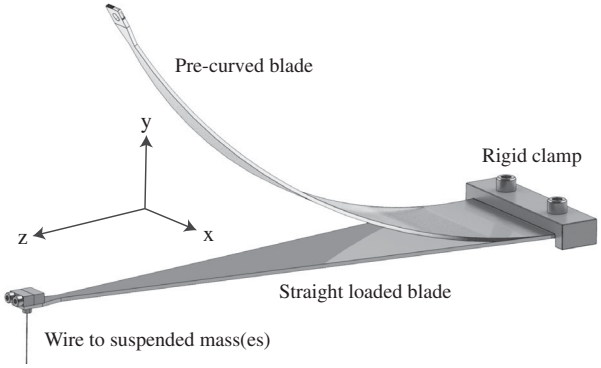

FIG. 2. An example of the metallic cantilevers considered in this paper. The blade is rigidly clamped at its base, precurved, and it straightens when a load is applied on the blade tip.

steel cantilever is rigidly clamped at the wide end and is free to move under a static load suspended from the narrow end. The blade is subject to a time varying perturbation due to external forces and seismic induced motion of the attachment point, which can trigger crackling events due to the changing stress in the material. The most relevant observable of the system is the vertical displacement of the blade tip, since this is transmitted down to the test mass through the wire that connects the blade to the lower parts of the Advanced LIGO quadruple suspension system, as shown schematically in Fig. 1. We focus on the blades that suspend the lowest two stages from the upper intermediate mass (UIM), since there is little vertical attenuation below them. Any noise in the upper stage blades is further attenuated by the additional vertical isolation in the UIM stage.

The rate and amplitude of crackling events are believed to depend on the stress and stress rate in the material [20]. In the Advanced LIGO suspension, time-varying stress in the blade is driven by the low frequency (below 1 Hz) residual seismic motion. We therefore expect the typical signature of crackling to be a nonstationary noise, which have statistical properties varying in correlation with the slow change of the seismic motion of the blade attachment point.

The lack of theoretical models of crackling noise in the elastic regime inspired new experimental investigations that are being carried out in the LIGO Laboratory at Caltech. Details of this *crackling noise experiment* are described in [29]. Here it suffices to say that a direct measurement of the displacement of the blade tip due to crackling noise is being attempted. To accommodate the experimental setup into the available space, smaller scale maraging blades are used (length of about 10 cm instead of about 30 cm as in the full scale Advanced LIGO suspension system), loaded with a single mass suspended by a steel wire. It is therefore necessary to develop a model to scale up the results obtained in the test facility to the full scale system. This is the goal of the work presented here. In the next sections we will describe a phenomenological model obtained from

a set of simple generic assumptions, and how to integrate it into a model of the entire cantilever and its interaction with the full suspension system. In this paper we describe the details of the model used to describe crackling noise in the blades used in the Advanced LIGO suspension system. A similar approach can be used to derive the same kind of description for the crackling noise experiment. We simply state the results in that case, and the interested reader can refer to [30] for more details.

II. PHENOMENOLOGICAL MODEL OF CRACKLING NOISE

The microscopic model of crackling noise is built on four assumptions about the nature of the single crackling events:

(1) *Typical length scale and independency.* Each crackling event affects a region of the metal crystal lattice that, even though involving many atoms at once, is much smaller than the size of the blade itself. Even if we consider the possibility of avalanches of dislocation motion [12,13], the size of the region involved is microscopic. We therefore treat crackling events as localized releases of energy. Additionally, since the interaction length is much smaller than the blade size, events happening at macroscopically different positions in the blade are statistically independent.

(2) *Large number of events.* Given the Advanced LIGO sensitivity and the suspension performance, we mostly focus on the 10–100 Hz region. We assume that the rate of events is reasonably large on the characteristic time scale we are interested in, so that we cannot distinguish single crackling events but we only measure the incoherent sum of many of them in the form of random noise.

(3) *Elastic blade response.* Even though the microscopic behavior of the material shows deviation from linearity (otherwise there would be no crackling noise), we assume that on a macroscopic scale the response of the blade to excitation from isolated crackling events follows a simple linear elastic law.

(4) *Dependency on local properties.* We describe the rate and distribution of crackling events as local variables, which, however, are allowed to have different values in different points inside the blade. Those variables can depend only on local properties of the blade. Some of those properties are related to the material (Young modulus, yield stress, density of dislocation, etc.). Since all blades are made of the same uniform material, we can assume that those properties are constant from blade to blade. Based on the assumption of an average elastic behavior of the blade, the two variables that can affect the crackling noise rate and amplitude are the local stress and the local stress rate.

The first and second assumptions allow us to describe crackling noise in the Advanced LIGO suspension and in the crackling noise experiment, as the incoherent sum of the effect of a large number of localized events, following a Poissonian distribution with a rate $r(x, y, z)$ that depends on the position into the blade (z is the coordinate along the blade length, x is the transverse coordinate along the blade width, and y is along the blade thickness; see Fig. 2). We are interested in the motion of the test mass: the third assumption allows us to model it with the response $R(t, x, y, z)$ of the blade and suspended elements to a single, localized force with a (random) amplitude $f_0(x, y, z)$ and a time evolution $\chi(t)$. We assume that all crackling events have the same average time dependency, while the amplitude can vary. Therefore the power spectral density of the vertical test mass motion due to the incoherent sum of all crackling events can be written as [31]

$$S_{\mathrm{TM}}(\omega) = |\tilde{\chi}(\omega)|^2 \int_0^L dz \int_{-h/2}^{h/2} dy \int_{-b(z)/2}^{b(z)/2} dx \times 2r(z,x,y)\langle f_0(z,x,y)^2\rangle |\tilde{R}(\omega,z,x,y)|^2, \quad (1)$$

where the integration is performed over the entire blade length L, thickness h, and variable width $b(z)$, and $\langle f_0(z,x,y)^2\rangle$ denotes the average squared value of the crackling event amplitude, depending on the local statistics. $\tilde{R}$ and $\tilde{\chi}$ are the Fourier transforms of the corresponding time domain functions. The microscopic physics of crackling events is encoded in the product $C(z,x,y) = 2r(z,x,y)\langle|f_0(z,x,y)|^2\rangle$. The fourth assumption above implies that this *crackling noise coefficient* C depends on the coordinates only through the local stress $\sigma(z,x,y)$ and stress rate $\dot{\sigma}(z,x,y)$. In general, the functional dependency of C on σ and $\dot{\sigma}$ can be much more complex. However, the blades used in both the crackling noise experiment and the large quadruple suspension systems are operating close to the same fraction of the yield stress (about 50%). Therefore it is safe to assume that a power series expansion of C holds for both systems,

$$C \simeq C_0 + C_1\sigma + C_2\sigma^2 + C_3\dot{\sigma} + C_4\dot{\sigma}^2 + C_5\sigma\dot{\sigma}\cdots. \quad (2)$$

Since the thickness is significantly smaller than the length $b \ll L$, we can use the thin beam approximation [32,33]. The stress is therefore independent of the transverse coordinate x, and it has a linear dependency on y, measured with respect to the blade neutral midsurface. Therefore, when integrating over y in Eq. (1), only the terms proportional to σ^2, $\dot{\sigma}^2$, and $\sigma\dot{\sigma}$ survive. This leaves us with three coefficients C_2, C_4, and C_5 that encode the microscopic physics of crackling noise.

The total stress at each location in the blade has two components: a static part due to the initial precurvature and the static load that straightens the blade, and a time varying contribution due to either the motion of the blade attachment point due to residual seismic motion (in the Advanced

LIGO suspension) or the driving force applied to the tip of the blade (in the crackling noise experiment [29]). We will compute below both components using an elastic model of the blade.

III. ELASTIC MODEL OF THE CANTILEVER

Based on the third assumption, we can describe the blade as a linear elastic body. The blade is shaped like a trapezium, with length L, thickness h, and variable width $b(z) = b_0(1 - \beta z/L)$ where β is a shape factor, and b_0 is the major width. We describe the deformation of the blade with the displacement $w(z)$ of the median surface as a function of the coordinate z which runs along the blade length. The median is also a neutral surface of null stress. The only nonzero component of the stress is the zz component, which is given by [32,33]

$$\sigma_{zz} = -Ey\frac{\partial^2 w(z)}{\partial z^2}, \tag{3}$$

where E is Young's modulus of the material.

In the following sections we use a variational approach to derive the equilibrium position, the equations of motion, and the boundary conditions for the loaded blade, following the approach described in [33].

A. Equilibrium equation and static stress

The blade is clamped at its wide base, rigidly attached to the UIM stage of the suspension (Fig. 1), and a metal wire is used to suspend the lower elements of the system. However, to compute the static deformation of the blade under load, we can simply model the suspended elements with a total mass M_L concentrated at the blade tip. As shown in Fig. 2, the blade is initially curved with a radius R_0, and it deforms to a shape close to flat when loaded. Following [32,34], the potential energy of the system can be written as a function of the local angle $\theta(z)$ that the blade neutral surface forms with the z axis,

$$U[\theta(z)] = \int_0^L \left[I(z)\frac{E}{2}\left(\frac{d\theta}{dz} - \frac{d\theta_0}{dz}\right)^2 + M_L g \sin\theta(z)\right] dz, \tag{4}$$

where $I(z) = 1/12 b(z) h^3$ is the transverse momentum and $\theta_0(z) = z/R_0$ describes the unloaded circular shape of the blade. Requiring that the variation of the energy is zero with respect to the variable θ provides us with the equation of equilibrium and two boundary conditions,

$$\frac{d}{dz}\left[I\left(\frac{d\theta}{dz} - \frac{d\theta_0}{dz}\right)\right] - \frac{M_L g}{E}\cos\theta = 0, \tag{5}$$

$$\theta(0) = 0, \tag{6}$$

$$\frac{d\theta}{dz}(L) = \frac{1}{R_0}. \tag{7}$$

Since we already know that the equilibrium solution for a loaded precurved blade is very close to flat, we can use the approximation $|\theta| \ll 1$ to simplify and solve eq. (5) with the correct boundary conditions,

$$\theta_e(z) = \frac{L}{R_0}\frac{1-\beta}{\beta^2}\left[-\beta\frac{z}{L} - \log\left(1 - \beta\frac{z}{L}\right)\right], \tag{8}$$

with the additional condition that $R_0 = EI_0/gLM_L$. Here log denotes the natural logarithm. The static stress component can then be easily derived using Eq. (3).

B. Dynamical equations, time varying stress, and response to a single crackling event

To study the time-dependent response of the blade to an external disturbance (either the low frequency seismic motion or the localized crackling events) we need to build the full action for the system, which is composed of two parts: one related to the elastic deformation of the blade itself, and one related to the dynamics of the other suspension elements. If we describe the blade neutral surface position as a deviation from the equilibrium $w(z)$, relative to the blade clamp position, then the elastic potential energy is given by

$$U[w] = \int_0^L \left[\frac{EI}{2}\left(\frac{d\theta_e}{dz} - \frac{d\theta_0}{dz} + \frac{d^2 w}{dz^2}\right)^2\right] dz, \tag{9}$$

where we have neglected the gravitational potential energy of the blade, since it is typically small with respect to the elastic term and to the contribution coming from the suspended elements. The kinetic energy term for the blade is given by

$$T[w] = \int_0^L \frac{\rho A(z)}{2}\left(\frac{d(w + x_0)}{dt}\right)^2 dz, \tag{10}$$

where $A(z) = hb(z)$ is the blade transverse section area, ρ is the material density, and x_0 is the motion of the element where the blade base is attached. The work done by an external driving force with volume density $f(z)$ can be described by the additional term

$$F[w, t] = \int_0^L A(z) f(z) w(z) dz. \tag{11}$$

The term in the action that describes the blade is then simply given by the time integral of the above contributions

$$S_{\text{blade}}[w, \dot{w}] = \int_{t=t_1}^{t=t_2} (U[w] - T[\dot{w}] - F[w]) dt. \tag{12}$$

To obtain the equation of motion for the blade we need to compute the variation of this action with respect to the blade deformation $w(z)$. Using a sequence of integration by parts in both z and t, remembering that $\delta w(z,t_1) = \delta w(z,t_2) = 0$ and using the definition of the equilibrium position θ_e and of the initial curvature θ_0, it is straightforward to show that the equation of motion for the blade deformation is given by

$$EI(0)\left(1-\beta\frac{z}{L}\right)w'''' - EI(0)\frac{2\beta}{L}w''' + \rho A\ddot{w} = Af - \rho A\ddot{x}_0, \tag{13}$$

where w' denotes the derivative with respect to z and $\dot{w}$ derivative with respect to time. The integrations by parts leave some terms computed at $z = 0$ and $z = L$. Those terms, combined with the contributions from the variation of the action describing the suspended elements, provide the boundary conditions that the solutions must satisfy.

In order to correctly describe the dynamics of the blade, we need to include a model of the elements in the suspension chains that are above and below it.

In the general case, all the elements in the suspension system can be described as concentrated masses with appropriate moments of inertia and unidimensional elastic elements. Therefore we can describe the dynamics of the entire suspension, except for the blade, with an action which is a function of a set of generalized coordinates x_i. The suspension is connected to the blade only at the tip and at the base, so the suspension action will depend on the blade deflection only through $w(0)$ and $w(L)$. Therefore the variation of the action with respect to w will contain two terms connecting the blade with the dynamics of the suspension. Those terms will not influence the blade elastic equation for $w(z)$, but only the boundary conditions involving $w(0)$ and $w(L)$.

In the cases we are studying, to keep the model as simple as possible, but still capturing the vertical dynamics of the suspension, we made some simplifying assumptions, depicted in Fig. 3. First of all, we are interested in the motion of the lowest element in the suspension, the test mass. The motion of the blade tip due to crackling events is mostly vertical. The lower stages of the suspension are attached to two blades: therefore uncorrelated crackling events would generate an angular motion of the lower stages and of the test mass. However, because of the construction symmetry of the system, this motion would only excite the roll degree of freedom of the test mass (rotation around the interferometer laser beam axis) which is very weakly coupled to the gravitational wave signal and therefore can be neglected. Moreover, the suspension stages below the blades provide a large attenuation of all horizontal and angular motions. Therefore we can focus only on the vertical motion of all elements. The vertical motion of the test mass then couples to horizontal

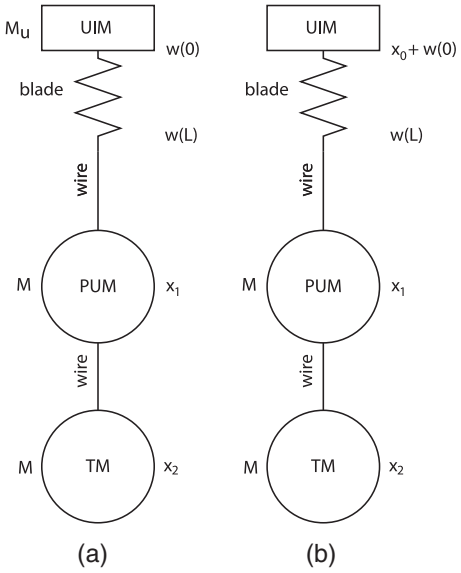

FIG. 3. Simplified models of the quadruple suspension system. In (a) the UIM stage is free to move, while in (b) its displacement is prescribed.

displacement mostly through the earth curvature over the interferometer 4-km-long baseline.

Additionally, the thin beam approximation we are using implies that we are ignoring the twisting modes of the blades, i.e. those that produce a rotation of the blade around the z axis. Although those modes could be excited by off centered crackling events, they have a much weaker coupling to the motion of the lower suspension stages, since the suspension wires are attached in a centered position on the blade tips.

We need to find the motion of the blade and of the suspended elements in two cases: (a) when the blade is subject to a localized crackling event, and (b) when the blade is driven by a prescribed motion of the base. In case (a) we want to describe the response of the test mass to a single crackling event, but we are interested only in a correct description in the observation band of Advanced LIGO, which is for frequencies above 10 Hz. Since all the upper stages of the suspension have resonant frequencies much below this by design, we can model the UIM (where the blade base is clamped; see Fig. 1) as a free mass and ignore again the dynamic of the stages above it. In this case we absorb the UIM motion x_0 into the blade clamp position and allow $w(0) \neq 0$. In case (b), the typical residual seismic motion of the UIM stage in the Advanced LIGO suspension is concentrated at very low frequencies (100 mHz), well below all resonances of the upper stages of the suspension. Therefore we can simply prescribe the motion x_0 of the blade base and ignore the dynamic of the upper suspension. In this case we enforce $w(0) = 0$.

Assuming that each of the suspension wires behave as a simple spring, with stiffnesses k_1 and k_2, it is straightforward to write the potential and kinetic energies of the suspension in the cases under analysis,

$$
\begin{aligned}
U^{(a)}_{\mathrm{susp}}[w(0), w(L), x_1, x_2] &= M_u g w(0) + Mg(x_1 + x_2) \\
&\quad + \frac{1}{2} k_1 [w(L) - x_1]^2 \\
&\quad + \frac{1}{2} k_2 [x_2 - x_1]^2, \\
K^{(a)}_{\mathrm{susp}}[\dot{w}(0), \dot{x}_1, \dot{x}_2] &= \frac{1}{2} M_u \dot{w}(0)^2 + \frac{1}{2} M(\dot{x}_1^2 + \dot{x}_2^2), \\
U^{(b)}_{\mathrm{susp}}[x_1, x_2, w(L)] &= Mg(x_1 + x_2) \\
&\quad + \frac{1}{2} k_1 [w(L) - x_1]^2 \\
&\quad + \frac{1}{2} k_2 [x_2 - x_1]^2, \\
K^{(b)}_{\mathrm{susp}}[\dot{x}_1, \dot{x}_2] &= \frac{1}{2} M(\dot{x}_1^2 + \dot{x}_2^2).
\end{aligned}
$$

In both cases we measure the coordinates from the equilibrium positions. The expressions above can be added to the expression of the action already derived for the blade. They contain terms dependent on the blade deformation at $z = 0$ and $z = L$, which contribute to the boundary conditions that the solutions must satisfy. By computing the variation of the total action with respect to $w(z)$, we obtain the following four boundary conditions for case (a):

$$
\begin{aligned}
w'(0) &= 0, \\
w''(L) &= 0, \\
-\beta \frac{EI_0}{L} w''(0) + EI_0 w'''(0) + M_u \ddot{w}(0) &= 0, \\
(\beta - 1) EI_0 w'''(L) + k_1 (w(L) - x_1) &= 0,
\end{aligned}
$$

and similarly for case (b):

$$
\begin{aligned}
w'(0) &= 0, \\
w''(L) &= 0, \\
w(0) &= 0, \\
(\beta - 1) EI_0 w'''(L) + k_1 (w(L) - x_1) &= 0.
\end{aligned}
$$

In both cases the fourth boundary condition provides the link between the elastic dynamics of the blade and of the suspended elements. By computing the variation of the total action with respect to the variables x_i, we get a set of differential equations, where the forcing term is given by $w(L)$,

$$
Mg - k_1 (w(L) - x_1) + k_2 (x_1 - x_2) + M\ddot{x}_1 = 0, \tag{14}
$$

$$
Mg - k_2 (x_1 - x_2) + M\ddot{x}_2 = 0. \tag{15}
$$

We can solve those equations in the frequency domain, and therefore completely describe the behavior of the suspended elements. This allows us to write $w(L) - x_1$ as a function of $w(L)$ only, valid in both case (a) and case (b),

$$
\begin{aligned}
k_1 (w(L) - x_1) &= \frac{k_1 M\omega^2 (2k_2 - M\omega^2)}{-k_1 k_2 + (k_1 + 2k_2) M\omega^2 - M^2 \omega^4} w(L) \\
&= K(\omega) w(L),
\end{aligned}
$$

where the last equality defines the new quantity $K(\omega)$.

To find the response of the system to either seismic residual motion or a crackling event, we solve the inhomogeneous differential equation (13) as an expansion in eigenmodes,

$$
w(z, t) = \sum_{i=0}^{\infty} \alpha_i(t) w_i(z), \tag{16}
$$

where $w_i(z)$ are the solutions of the following eigenmode equation (subject to the correct boundary conditions stated above):

$$
EI(0) \left(1 - \beta \frac{z}{L}\right) w_i'''' - EI(0) \frac{2\beta}{L} w_i''' - \rho A \omega_i^2 w_i = 0. \tag{17}
$$

The blade elastic equation becomes

$$
\sum_{i=0}^{\infty} w_i (\omega_i^2 \alpha_i + \ddot{\alpha}_i) = \frac{f}{\rho} - \ddot{x}_0,
$$

which can be solved by a Fourier transform. We first define the force and seismic motion projection into the eigenmodes and the orthogonality matrix as follows:

$$
F_j = \int_0^L A(f - \rho \ddot{x}_0) w_j dz, \tag{18}
$$

$$
M_{ij} = \int_0^L \rho A w_i w_j dz. \tag{19}
$$

The eigenmodes are not orthogonal, due to the inhomogeneous boundary conditions [33], therefore M_{ij} is not diagonal. The blade displacement in response to a distributed force or to seismic motion can be written as

$$
w(z) = \sum_{i=0}^{\infty} \frac{1}{\omega_i^2 - \omega^2} [\mathbf{M}^{-1} \mathbf{F}]_i w_i(z), \tag{20}
$$

where the bold symbols denote matrices and vectors and the subscript i refers to the ith element of the vector obtained from the matrix product in square brackets. The orthogonality matrix can be computed in a closed form from the boundary conditions. The details are not reported here since they add little to the discussion. The interested reader can refer to [30] for more details.

IV. NUMERICAL SOLUTION OF THE EQUATIONS

Equation (13) cannot be solved analytically in the case of a trapezoidal blade. Therefore we resort to numerical methods. We first rewrite all the equations and the boundary conditions in terms of the dimensionless variable $u = z/L$. In this way the length of the blade is factored out explicitly. Then we note that the boundary conditions involve the blade displacements at both $u = 0$ and $u = 1$. To cope with this complication, we follow the method described in [35]. For an arbitrary frequency ω_i we can find the four independent solutions q_j of Eq. (13) that satisfy the following set of conditions at $u = 0$:

$$\begin{aligned}
&q_1 : q_1(0) = 1 \quad q_1'(0) = 0 \quad q_1''(0) = 0 \quad q_1'''(0) = 0,\\
&q_2 : q_2(0) = 0 \quad q_2'(0) = 1 \quad q_2''(0) = 0 \quad q_2'''(0) = 0,\\
&q_3 : q_3(0) = 0 \quad q_3'(0) = 0 \quad q_3''(0) = 1 \quad q_3'''(0) = 0,\\
&q_4 : q_4(0) = 0 \quad q_4'(0) = 0 \quad q_4''(0) = 0 \quad q_4'''(0) = 1.
\end{aligned}$$

The solution that satisfies our original boundary condition is a linear combination $w_i = \sum_{j=1}^{4} a_j q_j$. Substitution of this expression into the boundary conditions gives a set of four homogeneous equations in the four unknown a_i. This linear system has a nontrivial solution only if its determinant, which is a function of $q_j(0)$ and $q_j(1)$, is zero. This provides us the condition that must be satisfied for ω_i to be an eigenvalue. We use numerical methods to find the zeros of the determinant and therefore find the first few eigenvalues ω_i and corresponding eigenmodes w_i. We can then use Eqs. (14) and (15) to compute the vertical motion of the test mass. The first few eigenmodes for case (a) are shown in Fig. 4. Similar results are obtained for case (b), the main difference being the additional constraint of zero displacement of the blade for $z = 0$.

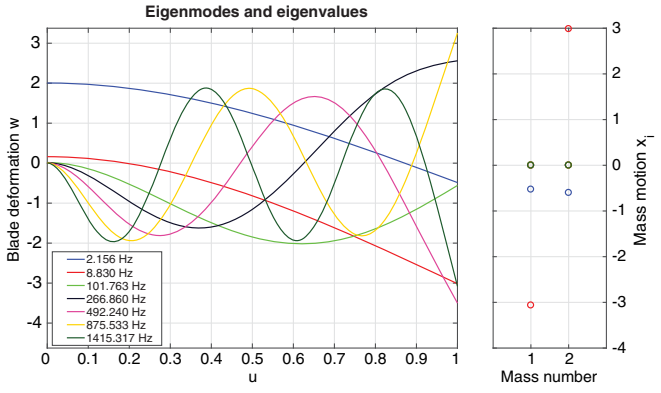

FIG. 4. The first few eigenmodes and eigenfrequencies for the system described in the text, in the case of a free UIM stage (case a). The left panel shows the blade deformation w for each mode, as a function of the dimensionless variable u. The right panel shows, on a different vertical scale, the corresponding motion of the suspended masses x_i, following the convention of Fig. 3. Units are arbitrary: the eigenmodes are normalized to unity mass, as defined by Eq. (19).

V. RESULTS

The numerical solutions described in the previous section allows us to compute all the components needed to derive an expression for the crackling-noise-induced vertical motion of the test mass. First of all, we need to compute the motion of the test mass due to a single crackling event in an arbitrary position z_0. We can use Eq. (20) and the following expression for a localized force:

$$f_0(z) = \frac{\delta(z - z_0)}{A(z_0)}. \tag{21}$$

The vertical motion of the test mass can then be computed using the result from Eq. (20) and the transfer function from the motion of the blade tip $w(L)$ to x_2, which can be computed from Eqs. (14) and (15),

$$T_2(\omega) = \frac{k_1 k_2}{k_1 k_2 - k_1 M\omega^2 - 2k_2 M\omega^2 + M^2\omega^4}. \tag{22}$$

This is a low pass filter with a corner frequency well below the range of interest for the crackling noise projections. Moreover, the only eigenmode that contributes significantly to the vertical motion of the test mass is the fundamental one, as apparent from Fig. 4. Therefore we can write the following approximated expression for the motion of the test mass due to a single crackling event in a position z_0 with unit amplitude, as defined in Sec. II:

$$\begin{aligned}
\tilde{R}(\omega, z_0) &= -\frac{T_2(\omega)}{\omega^2}\tilde{\chi}_0(\omega) w_0(L)\left(\sum_{i=0}^{\infty} M_{0i}^{-1} w_i(z_0)\right)\\
&= -\frac{T_2(\omega)}{\omega^2}\tilde{\chi}_0(\omega) w_0(L)\gamma(z_0),
\end{aligned}$$

where the last term in brackets defines the crackling noise coupling function $\gamma(z_0)$.

The second ingredient we need is the stress induced by the residual seismic motion of the blade attachment point. Again, we can compute it starting from Eq. (20) and the distributed force

$$f(z, t) = -\rho \ddot{x}_0(t). \tag{23}$$

Working in Fourier transform, we can write the projection of the force into the eigenmodes as

$$F_i(\omega) = \rho\omega^2 \tilde{x}_0(\omega) \int_0^L A w_i dz.$$

Next, we take into account that the residual seismic motion at the UIM stage is concentrated at low frequencies 200–100) mHz), lower than all eigenfrequencies. The fact that the load mass is much larger than the blade mass implies that the fundamental mode is a few hertz, while all higher modes are at much higher frequencies. This in turns implies that in the sum in Eq. (20), only the fundamental mode contributes significantly. Therefore we can write the

blade deformation in the form below, after going back to the time domain,

$$\begin{aligned} w(z) &\simeq \frac{1}{\omega_0^2}(\mathbf{M}^{-1}\mathbf{F})_i w_0(z) \\ &= -\frac{w_0(z)}{\omega_0^2}\rho\omega^2\ddot{x}_0\left(\sum_{i=0}^{\infty} M_{0i}^{-1}\int_0^L A w_i dz\right) \\ &= -\frac{w_0(z)}{\omega_0^2}\rho\omega^2\ddot{x}_0\Gamma, \end{aligned}$$

where the last term in brackets defines the seismic noise coupling coefficient Γ. From this result, the seismic induced stress can be computed using Eq. (3).

We can now substitute the results obtained in this section into the integral in Eq. (1) which gives us the total vertical displacement of the test mass due to crackling noise, using the definition of the crackling noise coefficients of Eq. (2). Since all numerical computations are performed in the dimensionless variable u, we recast all coefficients and integrals in terms of u, and factor out all the geometrical dimensions of the blade. The final result is given by

$$\begin{aligned} S_{TM}(\omega) = \frac{|\tilde{\chi}(\omega)T_2(\omega)|^2}{6\omega^4}\frac{b_0 h^3 w_0^2(L)E^2}{\rho^2 A_0^2}\cdot\Bigg[&\frac{\hat{I}_0}{LR_0^2}C_2 \\ &+\frac{\hat{I}_1\hat{\Gamma}}{L^3 R_0\omega_0^2}(2C_2\ddot{x}_0 + C_5\dddot{x}_0) \\ &+\frac{\hat{I}_2\hat{\Gamma}^2}{L^5\omega_0^4}(C_2\ddot{x}_0^2 + C_4\dddot{x}_0^2 + C_5\ddot{x}_0\dddot{x}_0)\Bigg], \end{aligned} \tag{24}$$

where we have defined the following quantities, which are all related to the eigenmodes and eigenfrequencies:

$$\begin{aligned} \hat{b}(u) &= 1-\beta u, \\ \hat{w}_i &= \int_0^1 du(1-\beta u)w_i(u), \\ \hat{M}_{ij} &= \int_0^1 du(1-\beta u)w_i(u)w_j(u), \\ \hat{\gamma}(u) &= \sum_{i=0}^{\infty}\hat{M}_{0i}^{-1}w_i(u), \\ \hat{\Gamma} &= \sum_{i=0}^{\infty}\hat{M}_{0i}^{-1}\hat{w}_i, \\ \hat{I}_0 &= \int_0^1 du\hat{b}(u)\hat{\gamma}^2(u)\left(\frac{1-u}{1-\beta u}\right)^2, \\ \hat{I}_1 &= \int_0^1 du\hat{b}(u)\hat{\gamma}^2(u)\frac{1-u}{1-\beta u}w_0''(u), \\ \hat{I}_2 &= \int_0^1 du\hat{b}(u)\hat{\gamma}^2(u)w_0''(u)^2. \end{aligned}$$

If the crackling noise coefficients C_k were known, Eq. (24) would provide us with an estimate of the test mass vertical motion.

As explained in the Introduction, since we are lacking a microscopical description of crackling events, we have developed an experimental setup, described in detail in [29], to measure the C_k for a smaller blade. The same approach described above can be used to obtain the expected scaling laws for crackling noise in this experimental setup. Apart from the blade dimensions, there are two notable differences. First, there is only one mass suspended from the blade tip: therefore the boundary condition equations and the dynamics of the suspended elements are different. Second, instead of considering the noise modulation due to residual seismic motion, we can apply a controlled sinusoidal excitation to the blade tip, with amplitude F_0 and frequency Ω. The same approach described above can be used to compute the total vertical motion of the experiment test masses due to crackling noise. The detailed computations are not reported here, and the interested reader can refer to [30]. The result is

$$\begin{aligned} S_{\text{vertical}}(\omega) = \frac{|\tilde{\chi}(\omega)T_1(\omega)|^2}{6\omega^4}\frac{w_0^2(L)h^3 b_0 E^2}{\rho^2 A_0^2}\Bigg[&\frac{\hat{I}_0}{R_0^2 L}C_2 \\ &+\frac{\hat{I}_1}{R_0 L^3}(-2C_2F_0 - C_5\dot{F}_0) \\ &+\frac{\hat{I}_2}{L^5}(C_2F_0^2 + C_4\dot{F}_0^2 + C_5F_0\dot{F}_0)\Bigg], \end{aligned} \tag{25}$$

where the same definitions used in the previous case hold, of course, using the eigenmodes and eigenvalues computed for the crackling noise experiment system.

VI. DISCUSSION

By combining Eqs. (24) and (25) with future results from the crackling noise experiment [29], we will be able to compute a projection of crackling noise for the quadruple suspensions used in Advanced LIGO. Since we still lack a microscopical description of the crackling events, we do not have any hint on the time evolution $\chi(t)$, which in turn means that we are missing the frequency dependency of the crackling noise. This frequency dependency will be another outcome of the experimental results.

However, we can estimate if the sensitivity of the crackling noise experiment described in [29] will be enough to detect crackling noise at a level which would provide meaningful noise projections for Advanced LIGO. We can start with the design sensitivity of the Advanced LIGO detectors, in the low frequency 10–30 Hz range. Assuming a coupling of vertical to horizontal motions of the test mass of about 10^{-3} (due to the earth curvature over the 4-km-long interferometer arms), and considering the cumulative effect of two blades for each of the four test masses, we can estimate that a vertical noise level of the order of 3×10^{-20} m at 20 Hz would result in a horizontal noise at the design sensitivity. The expected residual

TABLE I. Summary of the main mechanical and geometrical properties of the maraging blades used in the systems under consideration.

	Quadruple suspension blade	Crackling noise experiment blade
Length [mm] L	365	91
Maximum width [mm] b_0	49	18
Minimum width [mm] b_1	10	4.2
Geometry β	0.20	0.23
Thickness [mm] h_0	4.2	1.0
Mass [kg] m_B	0.294	0.008
Young's modulus [GPa]	186	
Density [kg/m^3]	8000	
	Quadruple suspension	Crackling noise experiment
UIM mass M_u [kg]	22	
Suspended masses M or m [kg]	39.7	2.2
Wire length L_1 [m]	0.34	0.15
Fiber length L_2 [m]	0.340	
Wire radius r_1 [mm]	0.60	0.5
Fiber radius r_2 [mm]	0.4	
Wire Young's modulus E_1 [GPa]	212	200
Fiber Young's modulus E_2 [GPa]	72	

seismic motion at the level of the UIM stage can be estimated to be of the order of 3×10^{-8} m, peaked at the microseismic frequency of about 200 mHz [36]. Using Eq. (24) and the parameters listed in Table I, we can translate this vertical noise into equivalent values for the crackling noise coefficients: $C_2 \sim 3 \times 10^{-36}$ Hz m, $C_4 \sim 4 \times 10^{-28}$ Hz^{-1} m, and $C_5 \sim 4 \times 10^{-36}$ m. Finally, we can use Eq. (25) and assume $F_0 \sim 10^{-3}$ N and $\Omega \sim 2\pi \times 0.1$ Hz to translate the estimate of the crackling noise coefficients (that would affect Advanced LIGO sensitivity) into the level of modulated noise to be detected in the crackling noise experiment. The results are of the order of 10^{-12} m$/\sqrt{\text{Hz}}$ for C_2 and C_4, and 10^{-8} m$/\sqrt{\text{Hz}}$ for C_5, all computed at 20 Hz. Those modulated noise amplitudes are well within reach of the experimental setup described in [29].

In conclusion, the model described in this work, although using a simplified description of the dynamic of the suspended element, is sufficient to capture the salient elements of how crackling noise scales with the dimension and geometry of the blades. When a suitable microscopic model of crackling events becomes available, it is straightforward to incorporate the predicted dependency of rate and amplitude on the stress and stress rate, thus directly predicting the level of crackling noise to be expected in Advanced LIGO. On the other hand, once data from the crackling noise experiment become available, the results described in this work will allow the computation of noise projections or upper limits for Advanced LIGO.

ACKNOWLEDGMENTS

LIGO was constructed by the California Institute of Technology and Massachusetts Institute of Technology with funding from the United States National Science Foundation under Grant No. PHY-0757058. The author would like to thank R. Adhikari (Caltech), K. Arai (Caltech), E. Gustafson (Caltech), X. Ni (Caltech), E. Quintero (Caltech), N. Robertson (Caltech), B. Shapiro (Stanford), B. Lantz (Stanford), and R. Weiss (MIT) for many useful discussions and suggestions. This paper has LIGO Document No. P1700072.

[1] G. Cagnoli, L. Gammaitoni, J. Kovalik, F. Marchesoni, M. Punturo, S. Braccini, R. De Salvo, F. Fidecaro, and G. Losurdo, Mechanical shot noise induced by creep in suspension devices, Phys. Lett. A **237**, 21 (1997).

[2] R. DeSalvo, Nonstochastic noise in gravitational wave detectors, in *Gravitational Waves, Second Amaldi Conference*, edited by E. Coccia, G. Veneziano, and G. Pizzella (World Scientific, Singapore, 1998), p. 228.

[3] S. Braccini *et al.*, Monitoring the acoustic emission of the blades of the mirror suspension for a gravitational wave interferometer, Phys. Lett. A **301**, 389 (2002).
[4] M. Biancolini, C. Brutti, G. Paparo, and A. Zanini, Fatigue cracks nucleation on steel, acoustic emission and fractal analysis, International Journal of Fatigue **28**, 1820 (2006).
[5] S. Braccini *et al.*, Measurement of the seismic attenuation performance of the Virgo superattenuator, Astropart. Phys. **23**, 557 (2005).
[6] M. Szabolcs *et al.*, Anatomy of the TAMA SAS seismic attenuation system, Classical Quantum Gravity **19**, 1605 (2002).
[7] M. V. Plissi, K. A. Strain, C. I. Torrie, N. A. Robertson, S. Killbourn, S. Rowan, S. M. Twyford, H. Ward, K. D. Skeldon, and J. Hough, Aspects of the suspension system for GEO 600, Rev. Sci. Instrum. **69**, 3055 (1998).
[8] M. Beccaria *et al.*, The creep problem in the Virgo suspensions: A possible solution using maraging steel, Nucl. Instrum. Methods Phys. Res. **404**, 455 (1998).
[9] N. Virdone, J. Agresti, A. Bertolini, R. DeSalvo, R. Stellacci, J. Kamp, M. Mantovani, V. Sannibale, M. Tarallo, and L. Kaltenegger, Extended-time-scale creep measurement on maraging cantilever blade springs, Nucl. Instrum. Methods Phys. Res. **593**, 597 (2008).
[10] R. Desalvo, Sz. Márka, K. Numata, V. Sannibale, A. Takamori, H. Tariq, E. J. Ugas, T. Yoda, Y. Aso, and A. Bertolini, Study of quality factor and hysteresis associated with the state-of-the-art passive seismic isolation system for gravitational wave interferometric detectors, Nucl. Instrum. Methods Phys. Res. **538**, 526 (2005).
[11] R. DeSalvo, A. DiCintio, and M. Lundin, The role of self-organized criticality in elasticity of metallic springs: Observations of a new dissipation regime, Eur. Phys. J. Plus **126**, 75 (2011).
[12] J. P. Sethna, K. A. Dahmen, and C. R. Myer, Crackling noise, Nature (London) **410**, 242 (2001).
[13] D. M. Dimiduk, C. Woodward, R. LeSar, and M. D. Uchic, Scale-free intermittent flow in crystal plasticity, Science **312**, 1188 (2006).
[14] N. Friedman, A. T. Jennings, G. Tsekenis, J.-Y. Kim, M. Tao, J. T. Uhl, J. R. Greer, and K. A. Dahmen, Statistics of Dislocation Slip Avalanches in Nanosized Single Crystals Show Tuned Critical Behavior Predicted by a Simple Mean Field Model, Phys. Rev. Lett. **109**, 095507 (2012).
[15] E. Vives, I. Ràfols, L. Mañosa, J. Ortín, and A. Planes, Statistics of avalanches in martensitic transformations. I. Acoustic emission experiments, Phys. Rev. B **52**, 12644 (1995).
[16] M.-C. Miguel, A. Vespignani, S. Zapperi, J. Weiss, and J.-R. Grasso, Intermittent dislocation flow in viscoplastic deformation, Nature (London) **410**, 667 (2001).
[17] J. Weiss, T. Richeton, F. Louchet, F. Chmelik, P. Dobron, D. Entemeyer, M. Lebyodkin, T. Lebedkina, C. Fressengeas, and R. J. McDonald, Evidence for universal intermittent crystal plasticity from acoustic emission and high-resolution extensometry experiments, Phys. Rev. B **76**, 224110 (2007).
[18] K. A. Dahmen, Y. B. Zion, and J. T. Uhl, Micromechanical Model for Deformation in Solids with Universal Predictions for Stress-Strain Curves and Slip Avalanches, Phys. Rev. Lett. **102**, 175501 (2009).
[19] P. D. Ispánovity, I. Groma, G. Györgyi, F. F. Csikor, and D. Weygand, Submicron Plasticity: Yield Stress, Dislocation Avalanches, and Velocity Distribution, Phys. Rev. Lett. **105**, 085503 (2010).
[20] R. A. White, Driving Rate Effects on Crackling Noise, Phys. Rev. Lett. **91**, 085702 (2003).
[21] S. M. Aston *et al.*, Update on quadruple suspension design for Advanced LIGO, Classical Quantum Gravity **29**, 235004 (2012).
[22] E. Hirose, T. Sekiguchi, R. Kumar, and R. Takahashi, Update on the development of cryogenic sapphire mirrors and their seismic attenuation system for KAGRA, Classical Quantum Gravity **31**, 224004 (2014).
[23] X. Ni, S. Papanikolaou, G. Vajente, R. X. Adhikari, and J. R. Greer, Probing Microplasticity in Small Scale FCC Crystals via Dynamic Mechanical Analysis, Phys. Rev. Lett. **118**, 155501 (2017).
[24] S. Braccini, C. Casciano, F. Cordero, F. Corvace, M. De Sanctis, R, Franco, F. Frasconi, E. Majorana, G. Paparo, and R. Passaquieti, The maraging-steel blades of the Virgo super attenuator, Meas. Sci. Technol. **11**, 467 (2000).
[25] J. Aasi *et al.* (LIGO Scientific Collaboration), Advanced LIGO, Classical Quantum Gravity **32**, 074001 (2015).
[26] K. Somiya *et al.* (KAGRA Collaboration), Detector configuration of KAGRA—the Japanese cryogenic gravitational-wave detector, Classical Quantum Gravity **29**, 124007 (2012).
[27] F Acernese *et al.* (Virgo Collaboration), Advanced Virgo: A 2nd generation interferometric gravitational wave detector, Classical Quantum Gravity **32**, 024001 (2015).
[28] Y. Levin, Creep events and creep noise in gravitational-wave interferometers: Basic formalism and stationary limit, Phys. Rev. D **86**, 122004 (2012).
[29] G. Vajente, E. A. Quintero, X. Ni, K. Arai, E. K. Gustafson, N. A. Robertson, E. J. Sanchez, J. R. Greer, and R. X. Adhikari, An instrument to measure mechanical up-conversion phenomena in metals in the elastic regime, Rev. Sci. Instrum. **87**, 065107 (2016).
[30] G. Vajente, LIGO Document No. T1700076, 2017, https://dcc.ligo.org/LIGO-T1700076.
[31] M. S. Bartlett, The spectral analysis of point processes, J. R. Stat. Soc. Ser. B **25**, 264 (1963).
[32] L. D. Landau and E. M. Lifshitz, *Theory of Elasticity (Volume 7 of A Course of Theoretical Physics)* (Pergamon Press, New York, 1970).
[33] S. S. Rao, *Vibration of Continuous Systems* (John Wiley & Sons, Hoboken, NJ, 2007).
[34] G. Cella, V. Sannibale, R. DeSalvo, S. Màrka, and A. Takamori, Monolithic geometric anti-spring blades, Nucl. Instrum. Methods Phys. Res., Sect. A **540**, 502 (2005).
[35] H. H. Mabie, and C. B. Rogers, Transverse vibrations of tapered cantilever beams with end loads, J. Acoust. Soc. Am. **36**, 463 (1964).
[36] F. Matichard *et al.*, Seismic isolation of Advanced LIGO: Review of strategy, instrumentation and performance, Classical Quantum Gravity **32**, 185003 (2015).